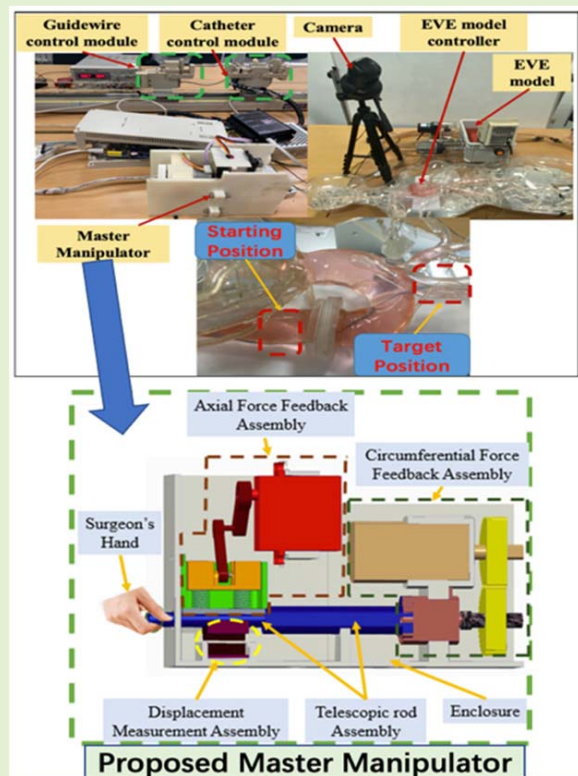


A Surgeon's Habits-Based Novel Master Manipulator for the Vascular Interventional Surgical Master-Slave Robotic System

Wei Zhou¹, Student Member, IEEE, Shuxiang Guo², Fellow, IEEE, Jin Guo,
Fanxu Meng, Student Member, IEEE, Zhengyang Chen,
and Chuqiao Lyu¹, Student Member, IEEE

Abstract—A master-slave vascular interventional surgical robotic system (MSVISRs) promises to treat cardio-cerebrovascular diseases without damaging the health of surgeons. Although many scholars are engaged in the research on the slave manipulator for the MSVISRs, there are very few studies on the master manipulator. In this study, a surgeon's habits-based novel master manipulator is developed. This master manipulator imitates the operating habits of surgeons in surgery and uses a non-contact method with an optical mouse sensor to measure the operating displacements. The novelty of this approach is that this master manipulator with smaller size and non-contact displacement measurement method can provide the axial force and the circumferential force feedback independently. In this master manipulator, the rigid-flexible coupling structure is used to provide the axial force feedback. In addition, the brush DC motor is used to give the circumferential force feedback. Furthermore, the proposed master manipulator is calibrated and evaluated by experiments. The calibration experiments show that the maximum identification ranges for the axial force and circumferential force in the proposed master manipulator are 0.247-4.5N and 0.52-4.3N, respectively. Moreover, the evaluation experiments show that the maximum error is 0.8 mm in the axial direction. As compared with other master manipulator, the comprehensive properties of this novel master manipulator are shown to be better and more promising.

Index Terms—Axial force feedback, circumferential force feedback, master manipulator, surgeon's habits, vascular interventional surgical robotic system.



Manuscript received February 24, 2022; accepted April 8, 2022. Date of publication April 11, 2022; date of current version May 13, 2022. This work was supported in part by the National Natural Science Foundation of China under Grant 61703305 and Grant 52005036, in part by the National High-Tech Research and Development Program (863 Program) of China under Grant 2015AA043202, and in part by Japan Society for the Promotion of Science (SPS) KAKENHI under Grant 15K2120. The associate editor coordinating the review of this article and approving it for publication was Prof. Kazuaki Sawada. (Corresponding author: Shuxiang Guo.)

Wei Zhou, Jin Guo, Fanxu Meng, Zhengyang Chen, and Chuqiao Lyu are with the School of Life Science, Beijing Institute of Technology, Beijing 100081, China.

Shuxiang Guo is with the Intelligent of Mechanical System Engineering Department, Kagawa University, Takamatsu 761-0396, Japan, also with the Key Laboratory of Convergence Medical Engineering System and Healthcare Technology, Ministry of Industry and Information Technology, Beijing Institute of Technology, Beijing 100081, China, and also with the Tianjin Key Laboratory for Control Theory and Application in Complicated Systems and the Intelligent Robot Laboratory, Tianjin University of Technology, Tianjin 300384, China (e-mail: guo.shuxiang@kagawa-u.ac.jp).

Digital Object Identifier 10.1109/JSEN.2022.3166674

I. INTRODUCTION

ACCORDING to the “World Health Statistics 2020” report by the World Health Organization, cardiovascular and cerebrovascular diseases have the highest mortality rates globally among patients dying from non-communicable diseases. Compared with open surgery, vascular interventional surgery (VIS) has advantages including relatively minor trauma, reduced bleeding and shorter postoperative recovery time. In a VIS, surgeons operate a catheter, guidewire, and other interventional surgical instrument to identify the location of a lesion and implement the planned treatments. Simultaneously, digital subtraction angiography (DSA) images provide guidance and assistance during the entire procedure. In a VIS, a surgeon's hand tremor (e.g., as caused by fatigue) will increase the risk of surgical failure, in addition, the X-ray radiation from the DSA and 20-kg lead clothing can

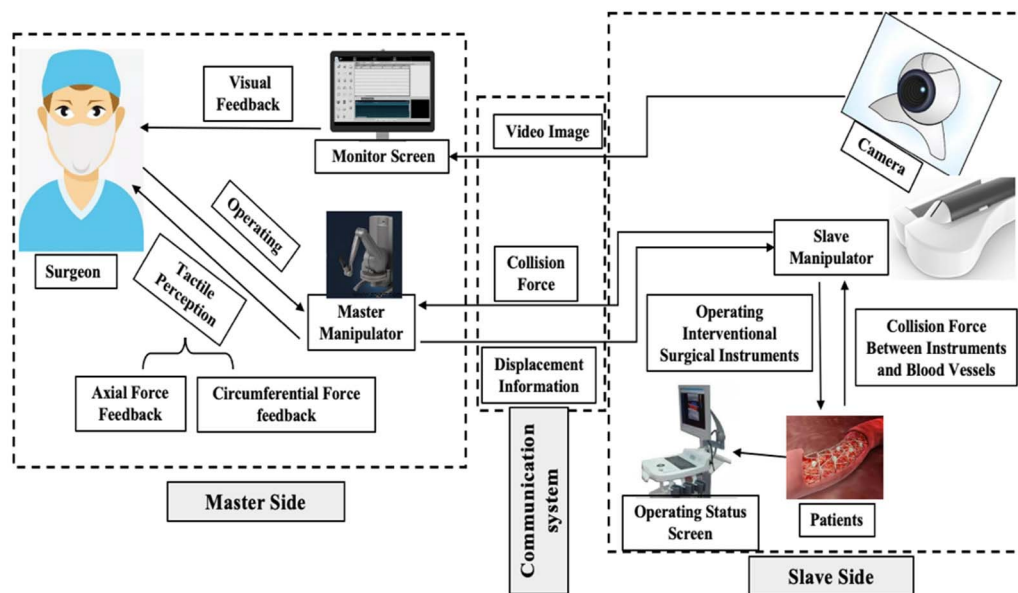


Fig. 1. Working principle of the master-slave robotic system.

increase the surgeon's risk of illness, leading to conditions such as spondylopathy and cancer. Therefore, a master-slave VIS robotic system is a promising and feasible solution for addressing the issues mentioned above. The working principle of the master-slave robotic system is shown in Fig. 1. The surgeon operates the master manipulator on the master side without X-ray radiation. A slave manipulator on the slave side is used to carry out the surgical operation. The communication system is the connector between the master and slave sides. In addition, the master manipulator generates the displacement information, which is transmitted to the slave manipulator to operate the surgical instruments through the communication system. In contrast, the slave manipulator collects the operating force between the surgical instruments and the vascular system and transmits this operating force to the master manipulator through the communication system, providing tactile perceptions to the surgeon. Moreover, a camera on the slave side is used to provide real-time images to a monitor screen on the master side, thereby providing visual feedback.

A. Related Works

Several advanced VIS robotic systems have been developed and commercialized, such as the CorPath[®] Robot System (Corindus Robotics Inc., Waltham, MA, USA) [1], Sensei[®] Robotic System (Hansen Medical Inc., Mountain View, CA, USA) [2], Amigo[®] Robot System (Catheter Precision Inc., Ledgewood, NJ, USA) [3], and Niobe (Stereotaxis Inc., St. Louis, MO, USA) [4]. Although the slave manipulators of these systems can operate the guidewire and the catheter, these robotic systems lack the tactile perception on the master manipulator. A lack of tactile perception is not conducive to the safety of surgical operations, as surgeons cannot create a sense of interaction in the surgical process as in real surgery.

Apart from these commercial systems, there are also some robotic systems in the experimental stage. Payne *et al.* proposed

a voice coil motor-based master manipulator for providing axial force feedback (AFF) [5]. Guo *et al.* developed a magneto-rheological fluids-based master manipulator, and the optical sensor was integrated to directly measure the displacement of the catheter. However, the size of the electromagnetic generator (which was used to control the magnitude of the feedback force) was too large to be convenient, and the accuracy of the displacement measurement was difficult to guarantee to a certain degree [6]–[8]. Jeon and Kim developed a magnetic micro active guidewire for reducing the operating time and improving the positioning accuracy; however, it was difficult to insert into cerebral, vascular, or other smaller-diameter vessels limited by their size [9]. Guo *et al.* developed a master manipulator for a novel system with haptic force feedback based on electromagnetic force. However, the contact displacement measurement influenced the accuracy of the force transmitted to the surgeon's hand [10], [11]. Bao *et al.* developed a cooperation mechanism for a catheter and guidewire in a VIS robotic system, and two commercial haptic devices (Geomagic@Touch X, 3D Systems, Inc., USA) were used as the master manipulator [12], [13]. He *et al.* developed a novel shape-memory polymer for active catheterization; the stiffness could be changed by using a water-cooling structure [14]. Wang *et al.* developed a system with 12 degrees of freedom and implemented four joysticks as the master manipulator, without force feedback [15]. Cha *et al.* developed a robotic system which adopted a stepping propulsion structure, and two pulleys were used to deliver a guidewire to a target position. In addition, multiple sleeves were used in the system to avoid bending of the guidewire and to ensure the displacement accuracy in the slave manipulator. In addition, a master manipulator with a telescopic parallel structure was developed, which provided AFF using DC motor; however, the operating handle was not a guidewire/catheter, so it was not in accordance with surgeons' operating habits [16]. Shen *et al.* developed a multifunctional

VIS robotic system able to realize guidewire driving, balloon catheter driving, and angiographic injector driving. The Omega 3, a commercial haptic handle, was implemented as the master manipulator, with force feedback. However, it failed to conform to the surgeon's clinical experience, increasing the operational time [17]. The proposed master manipulator only realized the AFF using a spring; this does not provide sufficient accuracy for the force feedback [18]. Shi *et al.* developed a VISRS with a haptic perception interface based on a spring-force generator to operate the catheter [19]. However, the circumferential force was not considered in this system. Meanwhile, there are also some studies from other fields that can help us to develop a novel master manipulator, such as the three-fingered force feedback glove [20], a pneumatic haptic device [21], and a haptic device based on an electrorheological actuator [22].

B. Challenges and Contributions

In general, there are very few studies on the development of a master manipulator able to provide the following three characteristics simultaneously: 1) the master manipulator can achieve both AFF and circumferential force feedback (CFF), and the haptic force is sufficiently large to be perceived; 2) the master manipulator implements a non-contact displacement measurement method with high performance; and 3) the master manipulator imitates the operating habits of surgeons in clinical surgery, and does not implement joysticks. In general, the meaning of "surgeon's habits" is that in a traditional clinical VIS, a surgeon operates the guidewire/catheter with three actions (push, retraction, and rotation along the axial direction), from the femoral artery to the target position [23]. To meet the above requirements simultaneously, there are two challenges for the research on master manipulators.

Challenge 1 concerns how to accurately and simultaneously measure the axial displacement and rotational displacement with the displacement measurement device (DMD) for the guidewire/catheter of the master manipulator. There are two reasons for this challenge. First, both the guidewire and catheter are too thin to measure the displacement accurately, which is terrible and unsafe for robot-assisted interventional surgery. In addition, because the guidewire (or catheter) can easily deform and has a certain deflection, there will be a more significant displacement measurement error, especially in the measurement of the axial displacement.

Challenge 2 concerns how to realize the AFF and the CFF simultaneously without interference. Notably, using only the axial force to provide the haptic force feedback is insufficient to some degree. The circumferential force is necessary for the actual feeling, but there is less corresponding research. Meanwhile, it is essential that there be no interference between the AFF and CFF, and that no interference influences the guidewire/catheter movement either. In addition, although the axial force can be used to identify the primary threats to puncturing vascular structures, the circumferential force is also necessary to provide the actual feeling. This is because surgeons operate a catheter according to the total force in

clinical surgery; this total force consists of the axial force and circumferential force simultaneously.

Considering the above challenges, one contribution of this study is the proposal of a surgeons' habits-based novel master manipulator with a rigid-flexible coupling structure. In this study, a non-contact method for measuring the displacement is proposed to improve the accuracy. Meanwhile, an AFF device using the rigid-flexible coupling structure and CFF device using a DC motor are proposed for providing the real tactile perceptions.

The remainder of this paper is organized as follows. In Section II, the details of the structure and working principle of the master manipulator are presented. Section III presents three experiments for calibrating the proposed master manipulator, including the CFF calibration experiments, AFF calibration experiments, and DMD calibration experiments. Section IV presents the evaluation experiments for the proposed master manipulator. At last, in Section V, the results of the evaluation experiments are discussed.

II. DETAILS OF THE PROPOSED MASTER MANIPULATOR

A. Structure and Manufacture of the Proposed Master Manipulator

In a master-slave VIS robotic system, there are two aspects that should be considered for the design of the master manipulator. One is a functional aspect. An accurate displacement measurement method and force feedback method are necessary for the novel master manipulator. The second aspect concerns the assembly and layout. The size and complexity of the structure for this novel master manipulator must be considered. If the master manipulator has a smaller size and more compact layout, it is more convenient and user-friendly for the surgeons to perform the surgery, even in a relatively small space. Moreover, it does not require large auxiliary equipment, such as an air pump or magnetic field generator.

Based on the above design ideas, the entire structure of the novel master manipulator is presented in Fig. 2. This master manipulator includes a CFF assembly, AFF assembly, optical mouse sensor for measuring the displacements, telescopic rod, and enclosure (for providing accurate installation locations for other parts). The AFF assembly includes a steering engine, connecting rod, plunger, and lead rail, along with springs and silicon rubber. The CFF assembly includes a brush DC motor, torque transmission shaft, driving gear, driven gear, and electromagnetic connector. The electromagnetic connector (G-J12, OGURA CLUTH CO., LTD., China) is used to control that the telescopic rod assembly and torque transmission shaft are connected or not. If this connector works, the telescopic rod assembly and torque transmission shaft are connected, and the CFF assembly will work. Moreover, this connector can make sure coaxially between the telescopic rod assembly and torque transmission shaft. Furthermore, the AFF assembly is a rigid-flexible coupling structure, and can ensure the continuity of the positive pressure. In addition, in the AFF assembly, the silicon rubber with the ability to deform is used to transform the positive pressure from the springs to the telescopic rod.

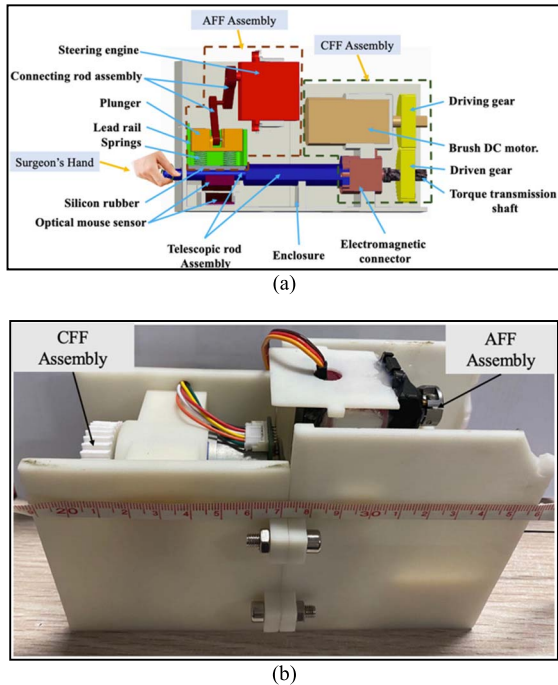


Fig. 2. Entire structure of the proposed master manipulator. (a) 3D model of the proposed master manipulator. (b) Manufacture and assembly of the proposed master manipulator.

Moreover, in the entire structure of the proposed master manipulator, the enclosure, torque transmission shaft, telescopic rod assembly, lead rail, plunger, driving gear, driven gear, and connecting rod are all manufactured by a 3D printer (iSLA660, ZRapid Tech) using a photosensitive resin material. In addition, the steering engine (DS3120, DSSERVO Inc., China) and brush DC motor (RS-455pa-18130, Mabuchi Motor, China) are applied to drive the AFF assembly and CFF assembly, respectively.

B. Working Principle of the Master Manipulator

Using the proposed master manipulator, a surgeon will hold the telescopic rod with the thumb, index finger, and middle finger. With the movement of the fingers, the telescopic rod will be pulled, retracted, or rotated along the axial direction. The pull and retraction actions are considered as one degree of freedom (DOF) for the straight motion, and the action of rotation is considered as one DOF of the rotating motion. Furthermore, the working principle of the master manipulator includes three states, which demonstrate that how the master manipulator works in the operation, including: (1) the displacement measurement with the AFF only, (2) the displacement measurement with the CFF only, and (3) the displacement measurement with both the AFF and the CFF. If the collision force is an axial force only, the case falls within the state (1). The state (1) in which the AFF assembly works is illustrated cooperatively by Fig. 2(a) and Fig. 3. The steering engine drives the connecting rod. Then, the plunger moves along the lead rail in the direction of gravity. The springs between the plunger and silicon rubber are compressed to gradually generate positive pressure. Then, the silicone rubber produces corresponding deformations according to the pressure, which

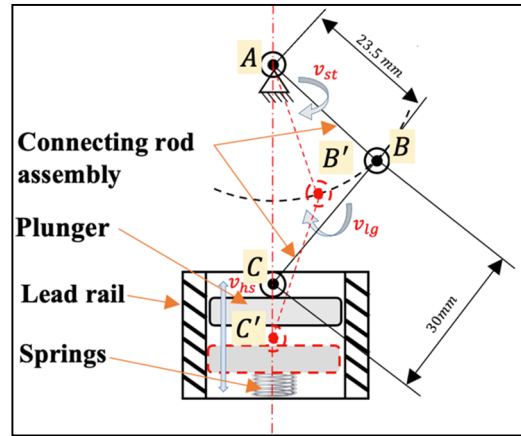


Fig. 3. Working principle of the axial force feedback (AFF).

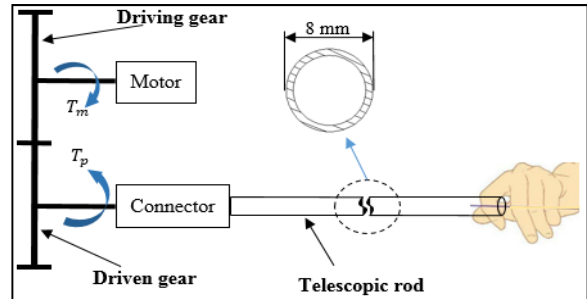


Fig. 4. Working principle of the circumferential force feedback (CFF).

is used to calculate the friction for the AFF. In contrast, when there is no axial force signal from the slave side, the AFF will disappear immediately. In contrast, if the collision force is the circumferential force only, the case falls within the state (2). The state (2) is illustrated cooperatively by Fig. 2(a) and Fig. 4. The electromagnetic connector is triggered to connect the torque drive shaft with the telescopic rod. Simultaneously, the brushless DC motor drives the driving gear by a motor shaft, and the driven gear drives the torque transmission shaft to generate the circumferential force. Regarding state (3), the AFF and CFF can be triggered simultaneously and independently.

III. CALIBRATION EXPERIMENTS FOR THE PROPOSED MASTER MANIPULATOR

Calibration experiments are necessary for developing this novel device. The objective of these experiments is to establish a mathematical model between the inputs and outputs in the control system. In the development of the master manipulator, the output comprises the feedback forces and displacements. In addition, the inputs include the voltage, angle, and pixel numbers. Therefore, the goals are to build three relationships. The first is to establish the relationship between the rotation angle of the steering engine and friction force; this relationship incorporates the silicon rubber applied to the telescopic rod. The second is to build the relationship between the torque and voltage; this is implemented to control the brush DC motor to provide the appropriate CFF. The third is to ensure the real resolution of the optical mouse sensor on the master manipulator.

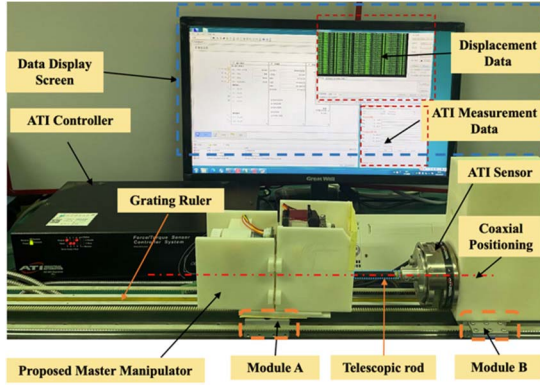


Fig. 5. Platform for the calibration experiments.

The calibration platform is presented in Fig. 5. The ATI sensor (Multi-Axis Force/Torque Sensor, ATI Industrial Automation, USA), which has high accuracy and sensitivity, is used to measure the AFF and CFF. Moreover, a grating ruler (GCXE-DK, Guiyang Xintian Optoelectronic Technology Co. Ltd, China) is used to measure the displacement of the DMD. In addition, when the calibration experiments are implemented, the ATI sensors are rigidly and coaxially connected with the telescopic rod of the master manipulator.

A. Calibration of the Axial Force Feedback (AFF)

When the calibration of the AFF is implemented, the mode of the ATI sensor will adjust to the force measurement mode based on the multi-axis force/torque sensor controller system. The proposed master manipulator is mounted on a Module A, and the ATI is mounted on a Module B, which is driven by the motor (525506, Maxon motor, Switzerland) through a synchronous belt at a constant speed. Module A and module B are coaxial assemblies on the same sliding rail. Furthermore, the rotational direction and speed of the motor are driven by the controller (ESCON 50/5, Maxon motor, Switzerland), as controlled by STM32 microcontrollers.

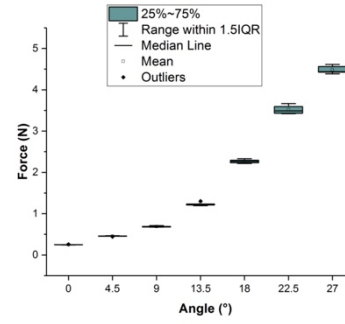
Therefore, when the steering engine rotates the different angles controlled by the STM32, including 4.5° , 9° , 13.5° , 18° , 22.5° , and 27° along the clockwise direction relative to the initial position, the module B will move to the module A. The corresponding friction will be recorded as shown in Fig. 6, i.e., the mean value of five times during the round trip with every angle. From the curve, we can obtain the proper relation between the rotation angle of the steering engine and friction force, shown in (1) as follows:

$$F_{axial} = -3 * 10^{-5} * X_{angle}^4 + 0.0015 * X_{angle}^3 - 0.0164 * X_{angle}^2 + 0.0946 * X_{angle} + 0.247 \quad (1)$$

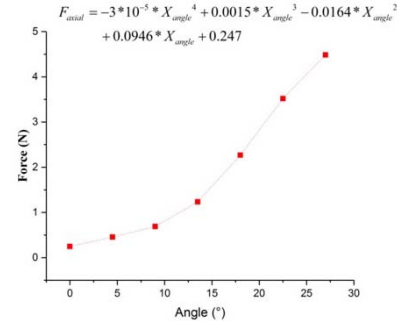
where F_{axial} denotes the axial force measured by the ATI sensor in the force measurement mode, and X_{angle} denotes the rotational angle generated by the steering engine.

B. Calibration of the Circumferential Force Feedback (CFF)

When the calibration of the AFF is implemented, the mode of the ATI sensor will adjust to the torque measurement mode



(a)



(b)

Fig. 6. AFF calibration experiments. (a) Axial force distribution of the five times experiments. (b) Fitted curve of the AFF calibration experiments based on the mean values.

based on the multi-axis force/torque sensor controller system. Unlike the calibration experiments of the AFF, in this case, both Module A and Module B are immobile. In addition, the rotational direction and speed of the brush DC motor are driven by the controller L298N, as controlled by STM32 microcontrollers. In addition, the on/ off state of the electromagnetic connector is controlled by the relay, which is also controlled by STM32 microcontrollers.

The experimental method comprises applying different voltages to the brush DC motor to obtain the corresponding circumferential force, including 1.07 V, 1.54 V, 1.98 V, 2.65 V, 3.17 V, 3.74 V and 4.28 V, and the recorded data shown in Fig. 7 represents the average value of five iterations. From the curve, we can obtain an accurate relation between the voltage and circumferential force, as shown in (2) as follows:

$$F_{cir} = 0.0162 * X_{cir}^3 - 0.1688 * X_{cir}^2 + 0.3853 * X_{cir} + 0.5242 \quad (2)$$

where F_{cir} refers to the circumferential force measured by the ATI sensor in the torque measurement mode, and X_{cir} is the voltage for controlling the DC motor.

C. Calibration of the Displacement Measurement Device (DMD)

The core component of the DMD is the optical mouse sensor chip (PAW3515DB-TJZA, PixArt Imaging Inc.). The resolution of this sensor is 1000 dpi, i.e., it can return 1000 coordinates per inch. In this study, the operational circuit of the data

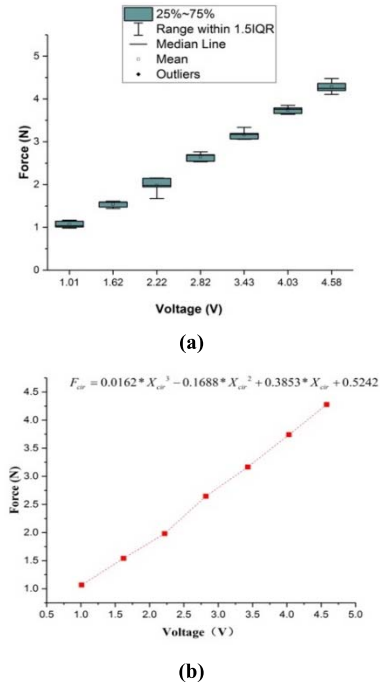


Fig. 7. CFF calibration experiments. (a) Circumferential force distribution of five iterations of experiments. (b) Fitted curve of the CFF calibration experiments based on the mean values.

processing chip of the DMD is redesigned according to the master manipulator design requirements. Only the axial and rotational displacement measurement functions of the optical mouse sensor are retained.

Furthermore, the calibration experiments of the DMD are implemented using the grating ruler. The grating ruler reading head is mounted on Module B. The proposed master manipulator is mounted on Module A to keep it immobile. When Module B moves to Module A, the number of coordinates and displacements of the grating ruler are recorded simultaneously; the details are shown in Fig. 8. From the curve, we can obtain an accurate relation between the displacements and pixel numbers. This relation is shown in (3) as follows:

$$L_{dis} = -3 * 10^{-9} * X_{dis}^3 + 5 * 10^{-6} * X_{dis}^2 + 0.032 * X_{dis} + 1.0568 \quad (3)$$

where L_{dis} refers to the displacements measured by the grating ruler, and X_{dis} is the numbers of pixel recorded by the optical mouse sensor.

IV. EVALUATION EXPERIMENTS FOR THE PROPOSED MASTER MANIPULATOR

A. Evaluation of the AFF and CFF

Here, the evaluation experiments for the accuracy of the AFF and CFF are discussed. The experimental platform is shown in Fig. 5. In this part, comparing to the calibration experiments, the proposed master manipulator is installed again, and the whole system is restarted. In addition, the operating method is the same with the calibration experiments in Part III. In the evaluation for the AFF, when the steering engine rotates the different angles controlled by the STM32, including

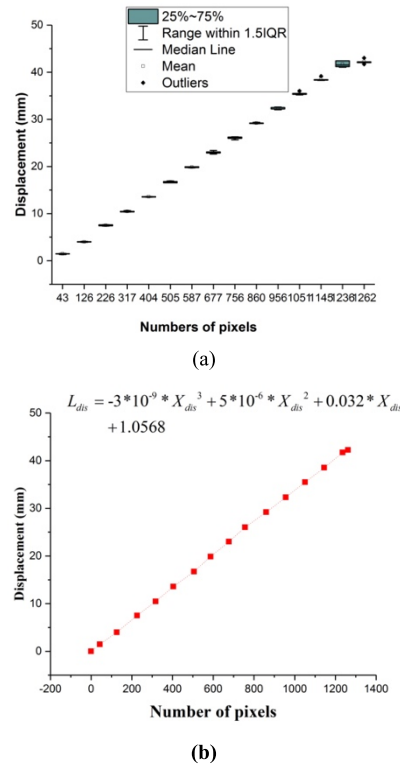


Fig. 8. Displacement measurement device (DMD) calibration experiments. (a) Displacement distribution of five iterations of experiments. (b) Fitted curve of the DMD calibration experiments based on the mean values.

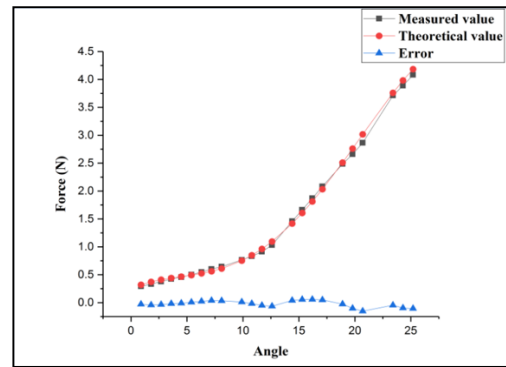


Fig. 9. Evaluation experiments for the AFF.

25.2°, 24.3°, 23.4°, 20.7°, 19.8°, 18.9°, 17.1°, 16.2°, 15.3°, 14.4°, 12.6°, 11.7°, 10.8°, 9.9°, 8.1°, 7.2°, 6.3°, 5.4°, 4.5°, 3.6°, 2.7°, 1.8°, 0.9° along the clockwise direction relative to the initial position, the module B will move to the module A. In the evaluation for the CFF, the experimental method comprises applying different voltages to the brush DC motor to obtain the corresponding circumferential force, including 4.44 V, 4.16 V, 3.91 V, 3.66 V, 3.18 V, 2.94 V, 2.69 V, 2.46 V, 1.97 V, 1.74 V, 1.47 V, 1.24 V, 0.88 V, and 0.77 V. The measured values, which are measured by the ATI sensor, are generated using the mean values in increasing and decreasing directions, and every mean value is calculated by three times in every direction.

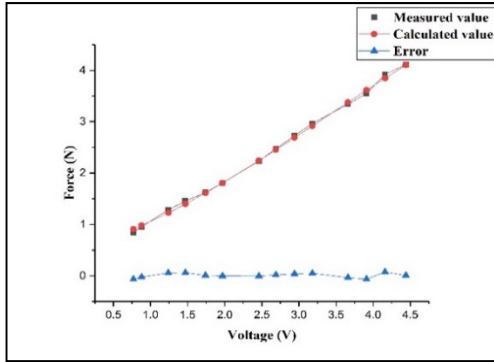


Fig. 10. Evaluation experiments for the CFF.

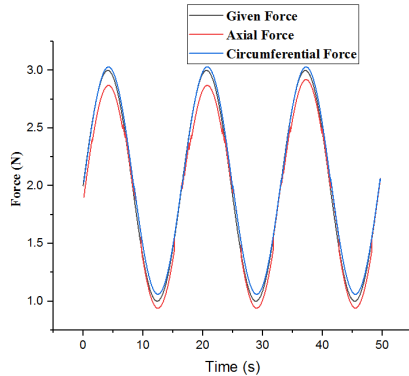


Fig. 11. Operating force based sinusoidal force command.

Moreover, in this part, the time-based response experiments, which are activated by a sinusoidal force command, are demonstrated to evaluate the dynamic response characteristics. The sinusoidal force command is illustrated by the equation (4). In addition, this force command is the input for the AFF and CFF assembly simultaneously, and the sample time is 33ms.

$$F_{given} = \sin\left(\frac{4\pi}{33}t\right) + 2 \quad (4)$$

where the F_{given} is the given force for the force feedback.

The evaluation experimental results are shown in Fig. 9, 10 and 11. Fig. 10. In Fig. 9, the maximum and mean errors are 0.15 N and 0.046 N, respectively. The minimum identifiable force of the AFF is 0.247 N. In Fig. 10, the maximum and mean errors are 0.063 N and 0.030 N, respectively. The minimum identifiable force of the CFF is 0.524N. In the Fig. 11, the delay time is 99 ms between the given force and measured force. The maximum and minimum errors are 0.12N and 0.03N, respectively. In addition, the frictional nature of the mechanisms maybe cause the hysteresis behavior. Moreover, the hysteresis behavior observed is also related to the manufacturing accuracy of the components.

B. Evaluation the Proposed Master Manipulator Through Master-Slave Robotic System

In this part, the purpose of the experimental experiments is to evaluate the performance of the proposed master manipulator through the given target using an endovascular evaluator (EVE, Fain-biomedical, Nagoya, Japan), which can simulate

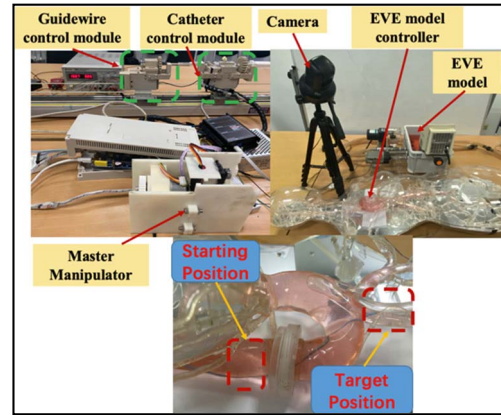


Fig. 12. Platform for the evaluation experiments.

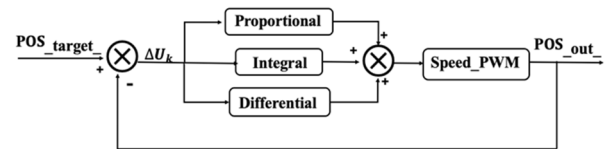


Fig. 13. Incremental proportional-integral-derivative (PID) control algorithm.

the surgical environment. The experimental setup for the evaluation experiments is shown in Fig. 12, and consists of the slave manipulator proposed in [12], a camera used to provide the images during the operation, EVE model used to conduct the experiments, and an EVE model controller used to circulate the fluids injected into the EVE model.

In addition, this slave manipulator has two modules(catheter control and guidewire control module)to clamp and operate the catheter and guidewire, respectively. The control method for the catheter control module is the same as that for the guidewire control module. Therefore, the experiments are implemented through the catheter control module, and the guidewire control module is omitted. The catheter control module is controlled in these experiments through an incremental proportional-integral-derivative (PID) control algorithm, as shown in Fig. 13. The POS_{target} is the target position of the catheter driver movement.

The Figs.14, 15 and 16 illustrate the experimental results of the axial displacements, circumferential displacements, and the operating forces, respectively. In the Fig.14 and Fig. 15, the errors between the theoretical values calculated by (3) and the actual measurement displacements are calculated through the encoder, based on 512 counts per turn of the linear-driven motor and rotary-driven motor. Fig. 16 illustrates the force values of the master and slave side, and the errors between them. In the slave side, the forces are measured by the force sensor in the catheter control module of the slave manipulator during the experiments. In the master side, the forces refers to the real forces that operator feels through the AFF assembly.

In Fig. 14, the maximum error is 0.8 mm in the axial direction. In a traditional VIS, if the movement error is less than 2 mm, we can consider that it is safe [7]. In Fig. 15, the maximum error is 15° in the circumferential direction. Although the more considerable error of the rotation cannot threaten safety, it is also necessary to improve the accuracy.

TABLE I
PERFORMANCE COMPARISON THE PROPOSED MASTER MANIPULATOR AND THE PREVIOUS STUDIES

Name	Volume size (mm^3)	LEDR (Yes/ No)	FC (Yes/ No)			AD (mm)	IRF (N)	
			DMD	AFF	CFF		AFF	CFF
Proposed master manipulator	$170 \times 66 \times 110$	No	non-contact	Yes	Yes	< 0.8	≥ 0.24	≥ 0.52
Omega 3 [17]	$270 \times 300 \times 350$	No	contact	Yes	No	< 0.01	Not clear	Not clear
Touch X [14], [15]	$400 \times 140 \times 240$	No	contact	Yes	No	> 0.023	1.75–7.9	1.75–7.9
Magneto-rheological fluid (MRF)-based [7]– [10]	$>300 \times 150 \times 400$	Magnetic field generator	non-contact	Yes	No	≤ 2	≥ 0.37	≥ 0.37
<ul style="list-style-type: none"> ➤ CFF: circumferential force feedback ➤ AFF: axial force feedback ➤ DMD: displacement measurement device ➤ LEDR: large external devices required 			<ul style="list-style-type: none"> ➤ FC: functional comprehensiveness, ➤ AD: accuracy of the displacement ➤ IRF: identification range of the force 					

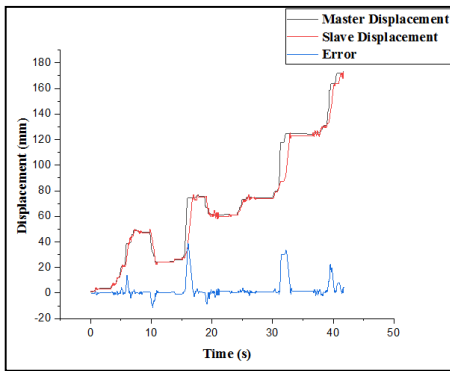


Fig. 14. Evaluation experiments for the DMD in the axial direction.

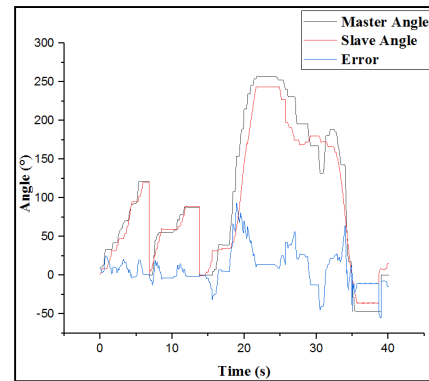


Fig. 15. Evaluation experiments for the DMD in the circumferential direction.

The error curves in Fig. 14 and Fig. 15 represent the real error at the same time, and demonstrate that the system’s response speed needs to be improved. Fig. 16 illustrates presents the operating forces in master and slave side during the experiments, and the maximum force error is 0.23N. In addition, the reason for very sharp drops and rises is not the instability issues of the controller but the intravascular environmental factors.

C. Comparison With Existing Master Manipulator

A performance comparison of the proposed master manipulator and an existing master manipulator is shown in TABLE I, including consideration of the volume size, large external devices required, functional comprehensiveness, coincidence with surgeon’s traditional operating habits, accuracy of the displacement, and identification range for the force. In addition, although some studies have used joysticks as the master manipulator [12]; these are not listed in TABLE I, because joysticks are not a competitive approach.

From comparison with the existing master manipulator, it can be seen that only the proposed master manipulator can meet the three characteristics in Section I. However, the precision for the AFF and CFF is less than that from the Omega 3 and Touch X, and is similar to precision of the

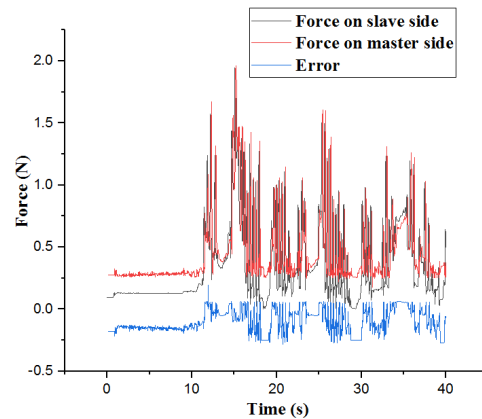


Fig. 16. Operating force during the operation.

magneto-rheological fluid-based master manipulator. In this research, the comprehensive performance refers to the four characteristics that should be considered in the development of the master manipulator, as mentioned in the Introduction section. Therefore, additional work should be performed to improve these two sections in the future, such as by using a high-precision stepping motor to replace the steering engine.

Moreover, we can analyze the results of the comparison in the context of the aspects of the application. It is easy to understand that the force is used to provide the tactile perception of an operation. Therefore, the most important is to generate a different feeling which can change through increasing and reducing the strength of the signal generated from the slave manipulator.

V. CONCLUSION AND DISCUSSION

This paper proposes a novel master manipulator with comprehensive functions, including AFF, CFF and non-contact displacement measured method. In addition, the AFF, CFF, and DMD are modularized, which is helpful in assembly, sterilization, and manufacture. Apart from those characteristics, the operating method of this proposed master manipulator is coincident with the surgeon's traditional operating habits in a VIS, and the size of the proposed master manipulator is smaller. Therefore, the proposed master manipulator is helpful for improving the performance of a master-slave robotic system. In [23], [24], many experiments were implemented to show that a master manipulator with force feedback can reduce the operation time.

From the calibration experiments, the data distributions are shown in Figs. 6(a), 7(a), and 8 (a), representing a better way to prove the robustness of the calibration equations. In addition, the maximum identification ranges of the axial force and circumferential force for the proposed master manipulator are 0.247 N–4.5 N and 0.52 N–4.3 N, respectively. Moreover, the evaluation experiments shows that the proposed master manipulator has the ability to help the operator to complete the target task.

Furthermore, when the surgical operation is proceeding, the on/ off of the DMD can be controlled by a button on the STM32, e.g., to reset the telescopic rod address and generate a continuous displacement. The above method is also adopted in the Touch X and Omega 3; thus, the proposed master manipulator can be updated easily. Because the AFF, CFF, and DMD are modularized, the maximum travel in every operation can be changed by simply modifying the length of the telescopic rod. This is a better approach to meeting the personalized requirements of surgeons.

In addition, coaxial positioning also plays a vital role in the development of the master manipulator, such as in the positioning relationships of the optical mouse sensor, telescopic rod assembly, and electromagnetic connector. Therefore, during the manufacturing process, it is necessary to ensure that the coaxial positioning relationship can accurately guarantee the operation accuracy of the master manipulator.

Moreover, with the catheter is inserted into the vascular deeper, the total force on the end side increases. Furthermore, environmental factors, such as heartbeats and the speed of the blood flow, can also influence the force on the end side. It is challenging to measure the total force directly, so the front side of the catheter is usually measured, which is similar to the operating of the surgeons. Moreover, the measured force is used for the surgeon by providing feedback. The actuator current will change when the length of the surgical tool inside the vascular structure increases. In addition, it is

considered that when the effort needed to drive the surgical tool increases, the actuator current will also increase. The force feedback to the master manipulator includes a collision force between the surgical tool and vascular wall, and a resistance force as generated by the water flow. The collision force will increase when the tip of the catheter deforms the vascular wall. The greater the vessel wall deformation, the greater the force produced. In addition, the force sensor in the slave manipulator only has the ability to measure the axial force for the catheter. Therefore, circumferential force is not presented in the experiments.

Moreover, This research adopts a real-time control strategy with an incremental PID control algorithm in the evaluation experiments, and the maximum delay time is less than 300 ms. However, the control method of this study is only the initial research, and algorithms with better real-time performance will be explored and applied, such as the adaptive disturbance rejection controller, which is promising for improving the accuracy and response speed [25].

REFERENCES

- [1] T. M. Patel *et al.*, "Comparison of robotic percutaneous coronary intervention with traditional percutaneous coronary intervention: A propensity score-matched analysis of a large cohort," *Circulat., Cardiovascular Interventions*, vol. 13, no. 5, pp. 1941–1963, May 2020.
- [2] C. V. Riga, C. D. Bicknell, A. Rolls, N. J. Cheshire, and M. S. Hamady, "Robot-assisted fenestrated endovascular aneurysm repair (FEVAR) using the Magellan system," *J. Vascular Intervent. Radiol.*, vol. 24, no. 2, pp. 191–196, Feb. 2013.
- [3] E. M. Khan *et al.*, "First experience with a novel robotic remote catheter system: Amigo mapping trial," *J. Intervent. Cardiac Electrophysiol.*, vol. 37, no. 2, pp. 121–129, 2013.
- [4] M. N. Faddis *et al.*, "Novel, magnetically guided catheter for endocardial mapping and radiofrequency catheter ablation," *Circulation*, vol. 106, no. 23, pp. 2980–2985, Nov. 2002.
- [5] C. J. Payne, H. Rafii-Tari, and G. Yang, "A force feedback system for endovascular catheterisation," in *Proc. IEEE/RJS Int. Conf. Intell. Robots Syst.*, Algarve, Portugal, Oct. 2012, pp. 1298–1304, doi: [10.1109/IROS.2012.6386149](https://doi.org/10.1109/IROS.2012.6386149).
- [6] S. Guo, Y. Song, and X. Yin, "A novel robot-assisted endovascular catheterization system with haptic force feedback," *IEEE Trans. Robot.*, vol. 35, pp. 685–696, Mar. 2019.
- [7] L. Zhang *et al.*, "Design and performance evaluation of collision protection-based safety operation for a haptic robot-assisted catheter operating system," *Biomed. Microdevices*, vol. 20, no. 2, pp. 1–14, Jun. 2018.
- [8] X. Yin, S. Guo, N. Xiao, T. Tamiya, H. Hirata, and H. Ishihara, "Safety operation consciousness realization of a MR fluids-based novel haptic interface for teleoperated catheter minimally invasive neurosurgery," *IEEE/ASME Trans. Mechatronics*, vol. 21, no. 2, pp. 1043–1054, Apr. 2016.
- [9] G.-H. Jeon and S. H. Kim, "Development and verification of mechanism for enhancement of steering angle and active locomotion for magnetic micro active-guidewire," *IEEE Access*, vol. 8, pp. 31103–31113, 2020, doi: [10.1109/ACCESS.2020.2973341](https://doi.org/10.1109/ACCESS.2020.2973341).
- [10] J. Guo, X. Jin, S. Guo, and Q. Fu, "A vascular interventional surgical robotic system based on force-visual feedback," *IEEE Sensors J.*, vol. 19, no. 23, pp. 11081–11089, Dec. 2019, doi: [10.1109/JSEN.2019.2935002](https://doi.org/10.1109/JSEN.2019.2935002).
- [11] J. Guo, X. Jin, and S. Guo, "Study of the operational safety of a vascular interventional surgical robotic system," *Micromachines*, vol. 9, no. 3, p. 119, 2018, doi: [10.3390/mi9030119](https://doi.org/10.3390/mi9030119).
- [12] X. Bao, S. Guo, L. Shi, and N. Xiao, "Design and evaluation of sensorized robot for minimally vascular interventional surgery," *Microsyst. Technol.*, vol. 25, no. 7, pp. 2759–2766, 2019.
- [13] C. Yang *et al.*, "A vascular interventional surgical robot based on surgeon's operating skills," *Med. Biol. Eng. Comput.*, vol. 57, no. 9, pp. 1999–2010, 2019.
- [14] C. He, S. Wang, and S. Zuo, "A linear stepping endovascular intervention robot with variable stiffness and force sensing," *Int. J. Comput. Assist. Radiol. Surg.*, vol. 13, no. 5, pp. 671–682, May 2018.

- [15] K. Wang *et al.*, "Design and performance evaluation of real-time endovascular interventional surgical robotic system with high accuracy," *Int. J. Med. Robot. Comput. Assist. Surg.*, vol. 14, no. 5, p. e1915, Oct. 2018, doi: [10.1002/rcs.1915](https://doi.org/10.1002/rcs.1915).
- [16] H.-J. Cha, B.-J. Yi, and J. Y. Won, "An assembly-type master-slave catheter and guidewire driving system for vascular intervention," *Proc. Inst. Mech. Eng., H, J. Eng. Med.*, vol. 231, no. 1, pp. 69–79, Jan. 2017.
- [17] H. Shen, C. Wang, L. Xie, S. Zhou, L. Gu, and H. Xie, "A novel remote-controlled robotic system for cerebrovascular intervention," *Int. J. Med. Robot. Comput. Assist. Surg.*, vol. 14, no. 6, p. e1943, Dec. 2018.
- [18] K. Wang, X. Mai, H. Xu, Q. Lu, and W. Yan, "A novel SEA-based haptic force feedback master hand controller for robotic endovascular intervention system," *Int. J. Med. Robot. Comput. Assist. Surg.*, vol. 16, no. 5, pp. 1–10, Oct. 2020.
- [19] P. Shi *et al.*, "Design and evaluation of a haptic robot-assisted catheter operating system with collision protection function," *IEEE Sensors J.*, vol. 21, no. 18, pp. 20807–20816, Sep. 2021, doi: [10.1109/JSEN.2021.3095187](https://doi.org/10.1109/JSEN.2021.3095187).
- [20] Z. Wang *et al.*, "A three-fingered force feedback glove using fiber-reinforced soft bending actuators," *IEEE Trans. Ind. Electron.*, vol. 67, no. 9, pp. 7681–7690, Sep. 2020.
- [21] H. Su, W. Shang, G. Li, N. Patel, and G. S. Fischer, "An MRI-guided telesurgery system using a Fabry–Perot interferometry force sensor and a pneumatic haptic device," *Ann. Biomed. Eng.*, vol. 45, no. 8, pp. 1917–1928, Aug. 2017.
- [22] A. Mazursky, J.-H. Koo, and T.-H. Yang, "A compact and compliant electrorheological actuator for generating a wide range of haptic sensations," *Smart Mater. Struct.*, vol. 29, no. 5, May 2020, Art. no. 055028, doi: [10.1088/1361-665X/ab710c](https://doi.org/10.1088/1361-665X/ab710c).
- [23] X. Jin, S. Guo, J. Guo, P. Shi, T. Tamiya, and H. Hirata, "Development of a tactile sensing robot-assisted system for vascular interventional surgery," *IEEE Sensors J.*, vol. 21, no. 10, pp. 12284–12294, May 2021.
- [24] X. Jin *et al.*, "Total force analysis and safety enhancing for operating both guidewire and catheter in endovascular surgery," *IEEE Sensors J.*, vol. 21, no. 20, pp. 22499–22509, Oct. 2021, doi: [10.1109/JSEN.2021.3107188](https://doi.org/10.1109/JSEN.2021.3107188).
- [25] J. Han, "From PID to active disturbance rejection control," *IEEE Trans. Ind. Electron.*, vol. 56, no. 3, pp. 900–906, Mar. 2009, doi: [10.1109/TIE.2008.2011621](https://doi.org/10.1109/TIE.2008.2011621).



Wei Zhou (Student Member, IEEE) received the B.S. degree in mechanical engineering from Ludong University, Shandong, China, in 2015, and the M.S. degree in mechanical engineering from Dalian Jiaotong University, Liaoning, China, in 2018. He is currently pursuing the Ph.D. degree with the Beijing Institute of Technology, Beijing, China.

He has published four refereed journals and conference papers. He researches robotic catheter systems for biomedical applications.



Shuxiang Guo (Fellow, IEEE) received the Ph.D. degree in mechano-informatics and systems from Nagoya University, Japan, in 1995.

He is currently a Full Professor with the Faculty of Engineering and Design, Kagawa University, Takamatsu, Japan. He is also a Chair Professor with the Key Laboratory of Convergence Medical Engineering System and Healthcare Technology and the Ministry of Industry and Information Technology, Beijing Institute of Technology, Beijing, China. He has published approximately 500 refereed journals and conference papers. His current researches include biomimetic underwater robots, medical robot systems for minimal invasive surgery, micro catheter systems, micropump, and smart materials (SMA and IPMC) based on actuators. He is the Editor-in-Chief for the *International Journal of Mechatronics and Automation*.



Jin Guo received the Ph.D. degree in intelligent machine system from Kagawa University in 2015. He was a Research Fellow with the Department of Biomedical Engineering, National University of Singapore. He is an Assistant Professor with the School of Life Science, Beijing Institute of Technology, China. His research interests include soft robotics for healthcare and robotic surgery.



Fanxu Meng (Student Member, IEEE) received the B.S. degree in biomedical engineering from the School of Life Science, Beijing Institute of Technology, Beijing, China, in 2020, where he is pursuing the M.S. degree.

He has published one refereed journal and conference paper. His research interests include reinforcement learning, deep learning, and surgical automation.



Zhengyang Chen received the B.S. degree in electronic and information engineering from the Beijing Institute of Technology, Beijing, China, in 2019, where he is currently pursuing the M.S. degree.

He has published two refereed journals and conference papers. He researches robotic catheter systems for biomedical applications.



Chuqiao Lyu (Student Member, IEEE) received the B.S. degree in bioengineering and the M.S. degree in biomedical engineering from the Beijing Institute of Technology, China, in 2016 and 2019, respectively, where he is currently pursuing the Ph.D. degree.

He has published two refereed journals and conference papers. He researches robotic catheter systems for biomedical applications.